GEOPHYSICAL RESEARCH LETTERS, VOL. 33, L18809, doi:10.1029/2006GL026954, 2006

Effect of parameterized sub-grid-scale diffusions on the source-receptor relationship in the WRF model

Shu-Hua Chen[1] and Hsiao-ming Hsu[2]

Received 19 May 2006; revised 10 July 2006; accepted 15 August 2006; published 23 September 2006.

[1] To provide a quantitative assessment of the source-receptor relationship in an Eulerian framework, the method of artificially adding oscillatory signals with different frequencies to emission locations for a scalar is evaluated. Two-dimensional numerical experiments of nonlinear hydrostatic mountain waves with wave breaking were used. The scalar time series were collected at a number of downstream locations and decomposed into frequency space to identify their sources and to investigate the strength of those signals with respect to different diffusion schemes. Six experiments were conducted using three sub-grid eddy coefficients (a constant, a function of deformation, and a function of turbulence kinetic energy (TKE)) and two environmental wind conditions (shear and no shear). Simulated oscillatory signals were affected by parameterized sub-grid-scale diffusions. Signals experiencing more sophisticated eddy coefficients were better preserved than those with the simplest constant ones. The signals were shifted to higher frequencies when using the TKE scheme under a uniform wind environment.
Citation: Chen, S.-H., and H. Hsu (2006), Effect of parameterized sub-grid-scale diffusions on the source-receptor relationship in the WRF model, *Geophys. Res. Lett.*, *33*, L18809, doi:10.1029/2006GL026954.

1. Introduction

[2] Fine pollutant particles can be suspended in the air for a long time and be transported for a long distance. These airborne pollutants have significant impacts on human health, visibility, and atmospheric radiative processes. The uncertainty of the source-receptor relationships prevents correct decision-making to optimally improve air quality. With respect to the sophisticated chemistry involved in general, such relationships are indeed complex.

[3] *Hsu and Chang* [1987] demonstrated a simple signal technique to identify the source-receptor relationship in some advective and diffusive numerical experiments with simple chemistry. In their study, a small unique oscillatory signal was superimposed onto each emission source using a simple horizontal x–y two-dimensional (2D) Eulerian model. A constant eddy coefficient was used in their model. In general, the transport of those oscillations was very sensitive to the numerical model diffusion as well as to the model nonlinearity. The primary objectives of this investigation are to adapt the signal technique to a more realistic but still idealized atmospheric model and to examine the technique with respect to different sub-grid-scale eddy diffusion schemes. The atmospheric flow we are interested in is the classical turbulent flow on the lee side of a mountain below the self-induced critical level. Such nonlinear flow is the consequence of wave breaking under certain flow regimes when mountain waves are present [*Peltier and Clark*, 1979]. *Miles and Huppert* [1969] indicated that wave breaking may occur when the parameter Nh/U is greater than 0.85, where U, N, and h are the upstream mean wind speed, Brunt-Vaisala frequency, and mountain peak height, respectively. Below this critical level, either self-induced or specified [*Peltier and Clark*, 1979; *Clark and Peltier*, 1984; *Durran*, 1986; *Peltier and Scinocca*, 1990; *Scinocca and Peltier*, 1991], the flow on the lee side is quite turbulent. We would like to study how artificially emitted signals are affected by the turbulent flow under different parameterization schemes. In addition to the classical uniform upstream wind profile, we also examine the same profile with a low-level shear layer. To study the source-receptor relationship of a scalar in an idealized flow condition is the first step toward progress in understanding the processes or phenomena associated with such relationships in real atmospheric environments. Therefore, an idealized atmosphere configured within an advanced non-hydrostatic numerical model is utilized here.

[4] This paper is organized as follows. The numerical model description and experiment design are described in section 2. The results are discussed in section 3, and concluding remarks are given in section 4.

2. Model Description and Experiment Design

[5] The Weather Research and Forecast (WRF) model, a next generation state-of-science mesoscale numerical model, was chosen to examine this signal technique. The WRF model is a jointly developed model, and there are two different dynamical cores available within the WRF framework. In this study, the Advanced Research WRF core (ARW) version 2.0 [*Skamarock et al.*, 2001, 2005; *Michalakes et al.*, 2001] was adopted (for information on the WRF Model, see www.wrf-model.org). The governing equations of the ARW are written in flux form using terrain-following mass coordinates, and mass and dry entropy are conserved. Model differential equations are approximated by the Runge-Kutta third-order scheme in time and by the fifth and third order advection schemes in horizontal and vertical directions, respectively. An open (radiative) lateral boundary condition and a free-slip lower boundary condition are applied. For studying the signal propagation, a new mass-conserved scalar equation was introduced and

[1]Department of Land, Air, and Water Resources, University of California, Davis, California, USA.
[2]National Center for Atmospheric Research, Boulder, Colorado, USA.

0094-8276/06/2006GL026954$05.00

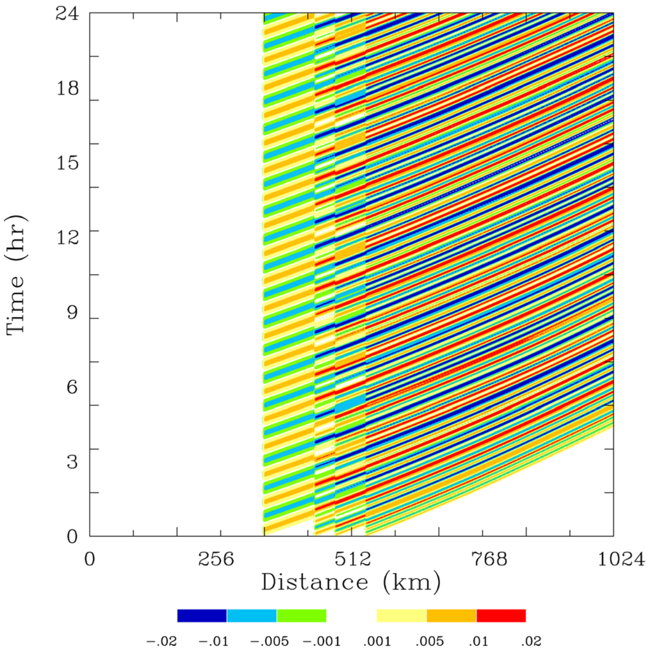

Figure 1. One day of time series data collected from the lowest level of the domain (512 grid points) during the second day of the ARW model simulation for the experiment with the use of the TKE scheme under the sheared environment.

implemented into the ARW. The new scalar was propagated and mixed as other scalars, such as water vapor, in the model.

[6] There are several idealized cases available from the ARW model. The two-dimensional (2D) mountain-wave case, which is conducted in a dry atmosphere, was selected and modified for our simulations. An idealized bell-shaped mountain was placed one fourth of the domain from the upstream boundary and the geometry was given as $h_s(x) = h / \{1 + [(x - x_0) / a]^2\}$, where $h_s(x)$, h, a, and x_o are the terrain height, the mountain peak (2 km), the mountain half-width (10 km), and the location of the center of the mountain, respectively. The horizontal domain size was 1024 km with a spatial resolution of 2 km, while in the vertical the grids were stretched with a total of 41 levels from 1000 hPa at the surface to about 50 hPa at the model top. The surface potential temperature was 288 K and the Brunt-Vaisala frequency was approximately 1×10^{-2} s^{-1}. The non-dimensional mountain height (Nh/U) was 2. The mountain waves remained hydrostatic since Na/U = 10, but the flow on the lee was expected to experience a hydraulic jump and become turbulent [*Lin and Wang*, 1996]. Three eddy viscosities of the sub-grid mixing were examined under two different vertical wind profiles: with and without wind shear. This gave a total of six experiments. The three eddy viscosities were defined as a) a constant (i.e., K theory; KT); b) a function of diagnosed deformation, using a Smagorinsky first-order closure approach (SMG) [*Smagorinsky*, 1963; *Deardorf*, 1972; *Moeng*, 1984; *Moeng and Wyngaard*, 1989]; and c) a function of predicted turbulence kinetic energy (TKE), which is from the TKE equation for the 1.5 Order Turbulence Closure [*Deardorf*, 1980; *Moeng*, 1984]. Detailed descriptions of those eddy viscosities can be found in *Skamarock et al.* [2005]. For experiments with a constant eddy viscosity, the horizontal and vertical coefficients for momentum variables were 30 and 3 m^{2}s^{-1}, respectively. The Prandtl number, which is defined as the ratio of the momentum viscosity to the thermal viscosity, was 1/3. For the no wind shear environment, a uniform mean wind of 10 ms^{-1} was used (i.e., a constant wind). For

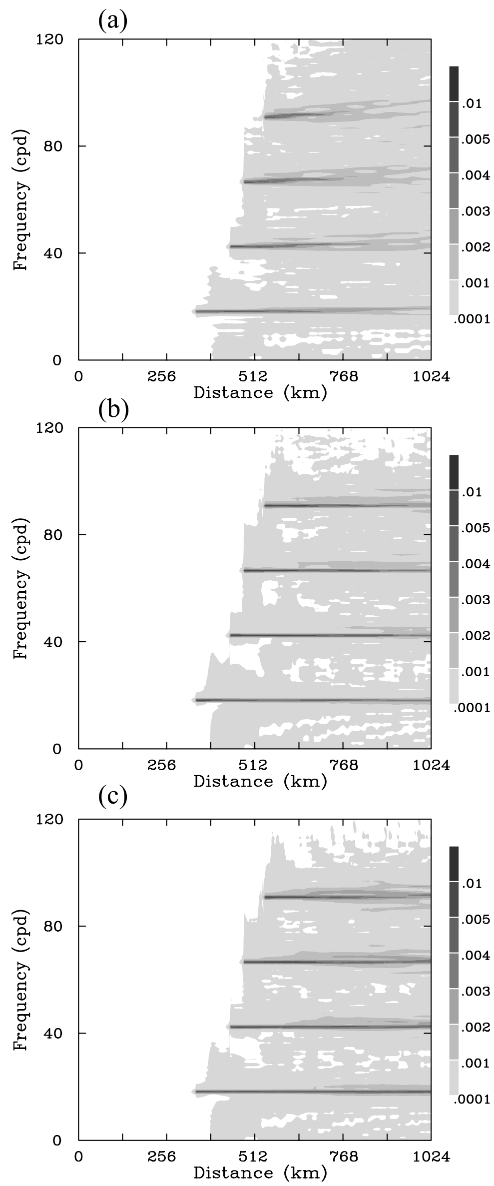

Figure 2. The amplitudes of frequencies (cycle per day) after applying a Fourier Transform to one day of time series data that were collected from the lowest level at each horizontal grid point (x-axis) for (a) K theory, (b) Smagorinsky, and (c) TKE sub-grid eddy diffusion schemes using initial conditions with the wind shear environment. The emission frequencies were 19, 43, 67, and 91 cycles per day from the surface at x = 342, 442, 482, and 542 km, respectively.

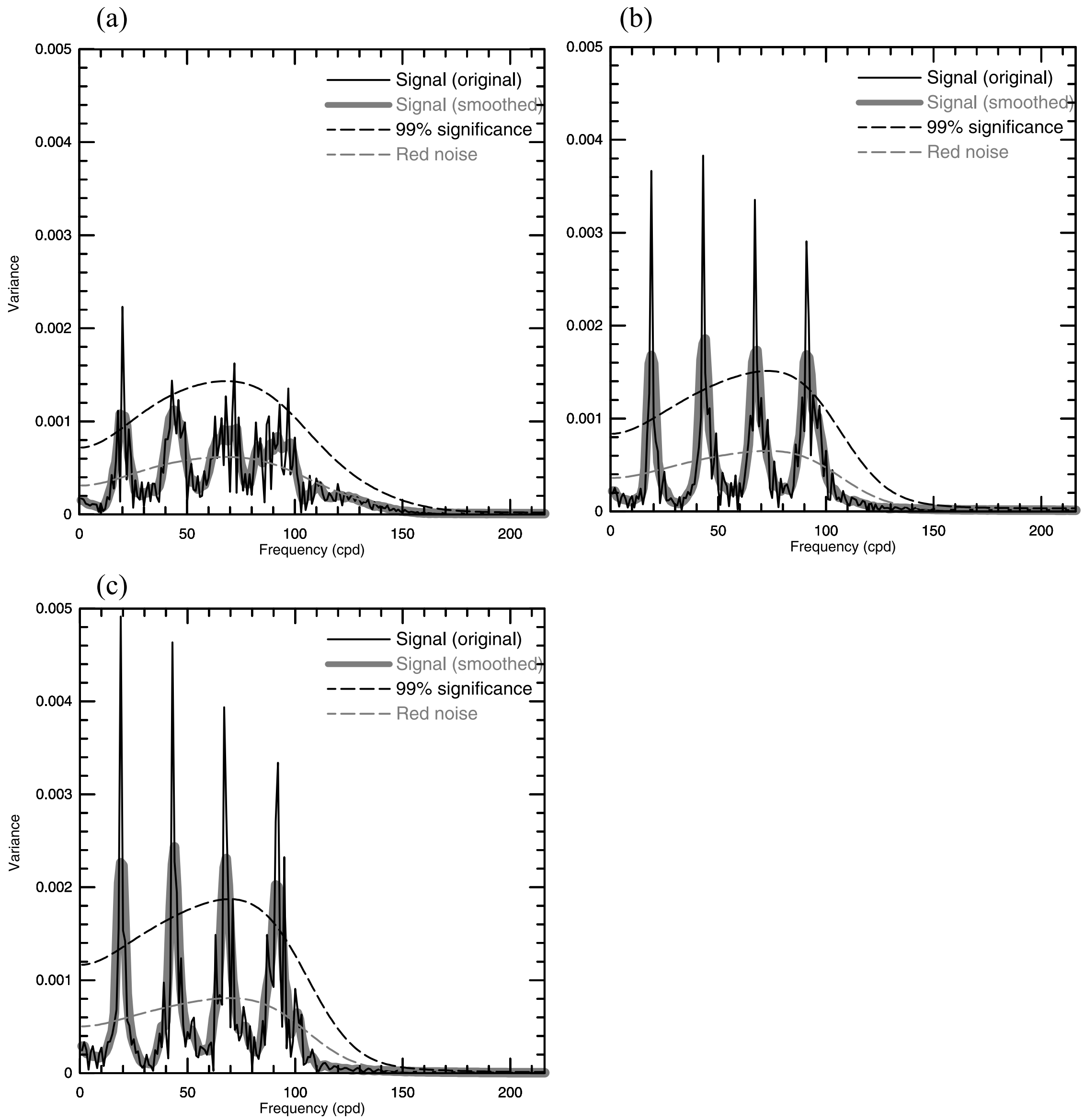

Figure 3. The temporal spectra of the scalar at the lowest level of the model at x = 1000 km for (a) K theory, (b) Smagorinsky, and (c) TKE sub-grid eddy diffusion schemes under the wind shear environment. The thin black lines are spectrally transformed from the original data set. The thick grey lines are spectra smoothed after one pass of the modified McDaniel filter. The gray dashed curves are the red spectra, and the black dashed curves indicate the 99% significance level. Emission frequencies were 19, 43, 67, and 91 cycles per day from the surface at x = 342, 442, 482, and 542 km, respectively.

the sheared environment, the wind was 15 ms^{-1} at the surface and linearly decreased with height to 10 ms^{-1} at 1.5 km height, then maintained a constant speed to the top of the domain.

[7] In each experiment, four oscillatory signals with different frequencies – 19, 43, 67, and 91 cycles per day – were constantly emitted from four different source points located at x = 342, 442, 482, and 542 km, respectively. The signals were released from the surface at the same time into the new scalar, called SIG, and were simulated for one day. Since the mountain was introduced impulsively into the background flow at the initial time, to avoid the initial shock and imbalance at the early simulation period, signals were released after one day of model simulations. The time step in ARW simulations was 20 seconds.

3. Results and Discussions

[8] The mountain waves in these simulations are hydrostatic and propagate vertically. As simulated signals mainly propagate near the surface for the given atmosphere here, SIG data at the lowest level of the domain (512 grid points) were collected for analysis. For example, Figure 1 shows the time series of SIG data from the experiment with the TKE viscosity under the sheared environment. One day of time series data collected at each point (e.g., vertical

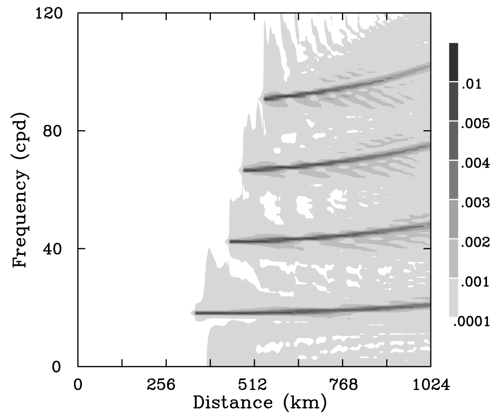

Figure 4. Same information as Figure 2c for the TKE eddy diffusion coefficient except under the no-shear environment.

columns of Figure 1) were then mapped onto the frequency space (cycles per day) using Fourier decomposition. In all experiments, four simulated signals propagated downstream to the lateral boundary before the end of the simulations (Figure 1). The signal from x = 542 km arrived at the lateral boundary about 5 hours after being released. Therefore, signals should be detected from the collected one-day SIG time series data at each grid point downstream of the emission source if there is no numerical error and if signals are not entirely diffused out.

[9] Figure 2 shows the amplitudes of frequencies (cycles per day) after the one-day SIG time series are Fourier-transformed under the low-level wind shear environmental condition. Four peak frequencies were clearly detected and mainly corresponded to those released upstream with each of the three eddy viscosities. Those signals collected from the lowest model level weakened, in particular with the use of constant eddy viscosities, when tracer propagated downstream since some are transported upward and some are diffused. The amplitudes at x = 1000 km, close to the downstream lateral boundary, are plotted in Figure 3 (thin black lines). The signals with SMG and TKE eddy viscosities are still clearly shown and exceed the 99% confidence level. However, the signals with constant viscosities (i.e., KT) became much weaker, in particular for the higher frequencies (i.e., 43, 67, and 91 cycles per day). High-order harmonics (HOH) due to aliasing and numerical schemes grew faster at the higher frequencies and the scenario with the KT eddy coefficient is the worst in this regard. For all simulations, the retrieved signals were more noticeable after one pass of the modified McDaniel filter [*Bloomfield*, 2000] (gray lines in Figure 3). Notably, the signals were preserved extremely well, especially when considering those that experienced a turbulent flow, rather than the constant flow of *Hsu and Chang* [1987].

[10] The results with different eddy viscosities under the no-shear environmental condition were very similar to those under the sheared environment, except for the experiment with the TKE eddy coefficient (Figure 4). The signals were still strong but the frequencies were shifted to higher numbers and the scenario worsened as the frequency increased. The HOHs also were worse than in the counterpart experiment with the sheared environment and the situation was more problematic with higher frequencies.

4. Concluding Remarks

[11] Using the Advanced Research WRF (ARW) model, experiments with an idealized 2D dry atmosphere and a mountain, which has a mountain peak of 2 km and a half-mountain width of 10 km, were conducted to study a signal technique. This signal technique can potentially be used to study the relationship between sources and sinks of scalars, such as water vapor and carbon dioxide, and the source-receptor relationship of pollutants. Six experiments were designed with the combination of three different eddy viscosities (a constant, a function of deformation, and a function of TKE) and two different vertical wind profiles (with shear and without shear). The signals propagated through the highly turbulent atmospheric flow produced by the nonlinear wave breaking on the lee side with the hydrostatic mountain waves. In each experiment, signals with four frequencies were released from different locations. Time series of the simulated data (SIG) at the lowest level of the model were collected and mapped onto the frequency space using Fourier transforms to illustrate the characteristics of signal propagation.

[12] Results from Fourier transform analysis show that each emitted signal with a unique oscillatory frequency could be detected downstream from the source points in all six experiments. The signals from experiments with Smagorinsky and TKE schemes were preserved very well after propagating downstream and the significance level of those signals reached 99%. However, signals from experiments with constant eddy viscosities became weaker and weaker when propagating away from the source points. Although the signals were weaker, distinct frequency peaks still were identifiable and could be used for practical applications. Moreover, high-order harmonics that were produced due to numerical aliasing and numerical methods became worse as the frequencies got higher; this was most noticeable when constant eddy viscosities were used. It was found that when the TKE viscosity was used under the no-shear environment, the simulated signals were shifted to higher frequencies and the effect was more pronounced as frequency increased. However, the signals were preserved quite well in the cases with the sheared environment.

[13] The preliminary results shown in this study are very encouraging and interesting. Of special interest is that the results with more sophisticated and realistic eddy viscosities (i.e., *Smagorinsky* [1963] and TKE schemes) are better than those with the simple approach (i.e., constant eddy viscosity). The signals with high frequencies were damped out faster (i.e., smoothed out) compared with those of low frequencies and higher frequency HOHs grew with time more quickly than lower ones. In order to optimize the use of this technique, more studies are required, such as using real case simulations, finding the upper bound of the frequency which might be environment related, studying the shift of frequencies, etc.

[14] **Acknowledgments.** This study is supported by NASA-NAG5-13678 project and NCAR Early Career Scientists Assembly.

References

Bloomfield, P. (2000), *Fourier Analysis of Time Series: An Introduction*, 2nd ed., 261 pp., Wiley-Interscience, Hoboken, N. J.

Clark, T. L., and W. R. Peltier (1984), Critical level reflection and resonant growth of nonlinear mountain waves, *J. Atmos. Sci.*, *41*, 3122–3134.

Deardorf, J. W. (1972), Numerical investigation of neutral and unstable planetary boundary-layers, *J. Atmos. Sci.*, *29*, 91–115.

Deardorf, J. W. (1980), Stratocumulus-capped mixed layers derived from a 3-dimensional model, *Boundary Layer Meteorol.*, *18*, 495–527.

Durran, D. R. (1986), Another look of downslope windstorms. 1. The development of analogs to supercritical-flow in an infinitely deep, continuously stratified fluid, *J. Atmos. Sci.*, *43*, 2527–2543.

Hsu, H.-M., and J. S. Chang (1987), On the Eulerian source-receptor relationship, *J. Atmos. Chem.*, *5*, 103–124.

Lin, Y.-L., and T. A. Wang (1996), Flow regimes and transient dynamics of two-dimensional stratified flow over an isolated mountain ridge, *J. Atmos. Sci.*, *53*, 139–158.

Michalakes, J., S.-H Chen, J. Dudhia, L. Hart, J. Klemp, J. Middlecoff, and W. Skamarock (2001), Development of a next generation regional weather research and forecast model, in *Developments in Teracomputing*: *Proceedings of the Ninth ECMWF Workshop on the Use of High Performance Computing in Meteorology*, edited by W. Zwieflhofer, and N. Kreitz. pp. 269–276, World Sci., Hackensack, N. J.

Miles, J. W., and H. E. Huppert (1969), Lee waves in a stratified flow. 4. Perturbation approximations, *J. Fluid Mech.*, *35*, 497–525.

Moeng, C.-H. (1984), A large-eddy-simulation model for the study of planetary boundary-layer turbulence, *J. Atmos. Sci.*, *41*, 2052–2062.

Moeng, C.-H., and J. C. Wyngaard (1989), Evaluation of turbulent transport and dissipation closures in second-order modeling, *J. Atmos. Sci.*, *46*, 2311–2330.

Peltier, W. R., and T. L. Clark (1979), Evolution and stability of finite-amplitude mountain waves. 2. Surface-wave drag and severe downslope windstorms, *J. Atmos. Sci.*, *36*, 1498–1529.

Peltier, W. R., and J. F. Scinocca (1990), The origin of severe downslope windstorm pulsations, *J. Atmos. Sci.*, *47*, 2853–2870.

Scinocca, J. F., and W. R. Peltier (1991), On the Richardson-number dependence of nonlinear critical-layer flow over localized topography, *J. Atmos. Sci.*, *48*, 1560–1572.

Skamarock, W. C., J. B. Klemp, and J. Dudhia (2001), Prototypes for the WRF (Weather Research and Forecast) model, paper presented at Ninth Conference on Mesoscale Processes, Am. Meterol. Soc., Ft. Lauderdale, Fla., 29 July to 2 Aug .

Skamarock, W. C., J. B. Klemp, J. Dudhia, D. O. Gill, D. M. Barker, W. Wang, and J. G. Powers (2005), A description of the advanced research WRF version 2, *NCAR Tech. Note, NCAR/TN—468+STR*, 100 pp., Natl. Cent. for Atmos. Res., Boulder, Colo.

Smagorinsky, J. (1963), General circulation experiments with the primitive equations. I. The basic experiment, *Mon. Weather Rev.*, *91*, 99–164.

S.-H. Chen, Department of Land, Air, and Water Resources, University of California, One Shields Avenue, Davis, CA 95616, USA. (shachen@ucdavis.edu)

H. Hsu, National Center for Atmospheric Research, P.O. Box 3000, Boulder, CO 80307-3000, USA.